

DEM-Based SAR Pixel-Area Estimation for Enhanced Geocoding Refinement and Radiometric Normalization

Othmar Frey, *Member, IEEE*, Maurizio Santoro, *Member, IEEE*, Charles L. Werner, *Senior Member, IEEE*, and Urs Wegmüller, *Senior Member, IEEE*

Abstract—Precise terrain-corrected georeferencing of synthetic aperture radar (SAR) images and derived products in range–Doppler coordinates is important with respect to several aspects, such as data interpretation, combination with other geodata products, and transformation of, e.g., terrain heights into SAR geometry as used in differential interferometric SAR (DInSAR) applications. For georeferencing, a lookup table is calculated and then refined based on a coregistration of the actual SAR image to a simulated SAR image. The impact of using two different implementations of such a simulator of topography-induced radar brightness, 1) an approach based on angular relationships and 2) a pixel-area-based method, is discussed in this letter. It is found that the pixel-area-based method leads to considerable improvements with regard to the robustness of georeferencing and also with regard to radiometric normalization in layover-affected areas.

Index Terms—Geocoding, radiometric calibration, terrain-based radiometric normalization.

I. INTRODUCTION

PRECISE terrain-corrected georeferencing of synthetic aperture radar (SAR) images and derived products in range–Doppler coordinates is relevant for data interpretation and for the combination with other geodata products. In addition, the transformation of data from map geometry to range–Doppler geometry is also very important, e.g., the transformation of terrain heights into SAR geometry as used in differential interferometric SAR (DInSAR) applications. A method for automated terrain-corrected SAR geocoding with a refinement step using a simulation of topography-induced radiometric features was described in [1]. The quality of the correlation-based geocoding lookup-table refinement is strongly dependent on the availability of distinctive common features in both the real SAR intensity image and its simulated counterpart. This SAR image intensity simulation makes use of the angular relationship between the surface normal of the local terrain patch and the range–azimuth geometry. This approach

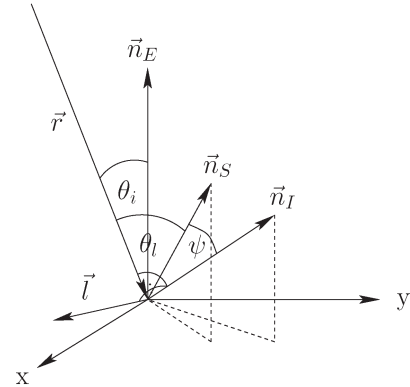


Fig. 1. Geometric relationships for angle-based simulations of illuminated area. \vec{r} : range vector (line of sight). \vec{l} : azimuth direction. \vec{n}_E : ellipsoid normal vector. \vec{n}_I : vector normal to image plane (normalized cross product of \vec{l} and \vec{r}). \vec{n}_S : normalized surface normal vector. θ_i : (ellipsoid-based) incidence angle. θ_l : local incidence angle. ψ : projection angle that relates the unit image area to the unit ground area when using the projection cosine approach (see also [4]).

and similar ones based on angular relationships were also assessed in [2] and [3]. In Fig. 1, the geometric definitions are given. This type of algorithm yields a realistic simulation of the terrain-induced variation of the backscattering coefficient, except for areas with strong foreshortening and layover regions, which notably are the most distinctive terrain-induced radiometric features.

A much better simulation of backscatter in layover regions is possible following ideas presented in [5]–[8], which have recently been summarized in [9]. We implemented such a digital elevation model (DEM)-based method for realistic SAR pixel-area estimation, and in this letter, we assess the improvement achieved in both the geocoding refinement and the radiometric normalization.

II. METHODS

A. Simulation of Illuminated Area

The radar brightness β^0 is defined as the average radar cross section per unit image area in range–azimuth coordinates. To obtain sensor-independent comparable measurements, the SAR image is commonly calibrated to σ^0 backscatter coefficients, which are defined as the average radar cross section per unit ground area, or to γ^0 backscatter coefficients, which are defined as the average radar cross section per unit area obtained by projecting the ground area into the plane perpendicular to the line of sight.

Manuscript received October 6, 2011; revised December 26, 2011 and February 27, 2012; accepted March 20, 2012.

O. Frey is with GAMMA Remote Sensing AG, 3073 Gümligen, Switzerland and also with the Earth Observation and Remote Sensing Group, Institute of Environmental Engineering, Swiss Federal Institute of Technology (ETH) Zurich, 8093 Zurich, Switzerland (e-mail: frey@gamma-rs.ch).

M. Santoro, C. L. Werner, and U. Wegmüller are with GAMMA Remote Sensing AG, 3073 Gümligen, Switzerland (e-mail: santoro@gamma-rs.ch; cw@gamma-rs.ch; wegmuller@gamma-rs.ch).

Color versions of one or more of the figures in this paper are available online at <http://ieeexplore.ieee.org>.

Digital Object Identifier 10.1109/LGRS.2012.2192093

Thus, in practice, the σ^0 and γ^0 average backscatter coefficients are obtained by relating the radar brightness β^0 to the respective reference areas A_{β^0} , A_{σ^0} , and A_{γ^0} as follows:

$$\sigma^0 = \beta^0 \frac{A_{\beta^0}}{A_{\sigma^0}} \quad (1)$$

$$\gamma^0 = \beta^0 \frac{A_{\beta^0}}{A_{\gamma^0}}. \quad (2)$$

For the standard ellipsoid-based products, the following simple trigonometric relationships involving only the incidence angle θ_i are valid:

$$A_{\sigma_{ell}^0} = \frac{A_{\beta^0}}{\sin(\theta_i)} \quad (3)$$

$$A_{\gamma_{ell}^0} = A_{\sigma^0} \cos(\theta_i) = \frac{A_{\beta^0}}{\tan(\theta_i)}. \quad (4)$$

Obviously, this approach yields inadequate estimates of the true ground area or the projected area in cases of rugged topography. In the following, two terrain-dependent methods to estimate the A_{σ^0} and A_{γ^0} reference areas are highlighted.

Projection Cosine Approach: Ulander [4] proposed a projection cosine method, which was applied for automated terrain-corrected SAR geocoding in [1]

$$A_{\sigma_{cos}^0} = \frac{A_{\beta^0}}{\cos(\psi)} \quad (5)$$

where ψ denotes the angle between the image plane normal and the surface normal, i.e., ψ relates the unit image area to the unit ground area. The respective $A_{\gamma_{cos}^0}$ reference area in the plane perpendicular to the line of sight is calculated via the cosine of the local incidence angle θ_l

$$A_{\gamma_{cos}^0} = A_{\sigma_{cos}^0} \cos(\theta_l). \quad (6)$$

This method is not well defined in layover areas as the underlying assumption of this method is a one-to-one correspondence between a slant-range position and a ground position [4]. It should be noted, however, that we calculate the projection cosine also in layover areas since it is still useful for geocoding purposes [1], whereas Ulander [4] explicitly excludes layover regions.

Pixel-Area Integration Method: In reality, many DEM pixels may contribute to a single range–azimuth coordinate. This is particularly the case in layover-affected areas. Therefore, a more realistic simulation of the topography-induced variation of radar brightness is obtained by integrating all DEM facets dA_{DEM} that contribute to a specific SAR pixel at range–azimuth coordinates (r, a) , i.e., that belong to the illuminated area, henceforth, termed pixel area A_{pa} . This idea was brought forward in [5]. In our implementation, the complete DEM surface covered by the SAR image is divided into small triangular surface patches dA_{DEM} , which are then “distributed” into range–azimuth “buckets,” i.e., the SAR pixels, according to the associated range–azimuth value as obtained from a geocoding lookup table. Note that the size of the triangular surface patches dA_{DEM} varies throughout the DEM. After having worked sequentially through all the rows and columns

(i, j) of the DEM, we end up with the sum of all contributing facets in each bucket, i.e., the total illuminated topographic area or *pixel area* $A_{\sigma_{\text{pa}}^0}$ for each pixel as follows:

$$A_{\sigma_{\text{pa}}^0}(r, a) = \sum_{i,j \in \mathcal{A}} dA_{\text{DEM}}(i, j) \quad (7)$$

where $\mathcal{A} := \{i, j | \rho(i, j) = r, \eta(i, j) = a\}$ and ρ and η are the range and azimuth values at DEM position (i, j) as obtained by bilinear interpolation of the lookup table and rounding to the next integer value. Similarly, the $A_{\gamma_{\text{pa}}^0}$ reference area is obtained via

$$A_{\gamma_{\text{pa}}^0}(r, a) = \sum_{i,j \in \mathcal{A}} [dA_{\text{DEM}}(i, j) \cdot \cos(\theta_l(i, j))]. \quad (8)$$

B. Geocoding Refinement

The SAR geocoding method described in [1] makes use of the satellite orbit, a digital terrain model, and the SAR imaging parameters to calculate the corresponding slant-range and along-track positions for each grid point of the digital elevation model. These initial slant-range and along-track positions are stored in a lookup table. As the next step, a simulated SAR intensity image is calculated. Then, offsets between the simulated image and the real SAR intensity image are determined and used to refine the lookup table. Eventually, the SAR image is transformed in one resampling step based on the refined lookup table. We compare the quality and robustness of this geocoding approach for the two different image simulation approaches: 1) the projection cosine-based approach; and 2) the pixel-area-based approach.

C. Radiometric Normalization

The terrain-corrected normalized backscatter coefficients σ_{cos}^0 and σ_{pa}^0 are obtained by inserting the reference areas $A_{\sigma_{\text{cos}}^0}$ from (5) and $A_{\sigma_{\text{pa}}^0}$ from (7), respectively, into (1). Similarly, the γ_{cos}^0 and γ_{pa}^0 backscatter coefficients are obtained using (6) and (8) in (2). In the following, the quality of the $\cos(\psi)$ -based radiometric normalization and the pixel-area-based radiometric normalization is assessed.

III. RESULTS

A. Geocoding Refinement

To demonstrate the increased robustness with respect to geocoding refinement provided by the new pixel-area-based SAR simulation, a subset of an European remote sensing satellite 2 (ERS-2) data set over the Mojave Desert in California is used. The area is mostly flat, only showing a very limited number of distinct topographic features (see Fig. 2). The second scene, also taken by ERS-2, shows an alpine area in southeastern Switzerland on the border to Italy (see Fig. 3). For the Mojave data set, the shuttle radar topography mission (SRTM) 1 arcsecond digital surface model is used. For the second example, the Swiss DHM25 digital elevation model is used, complemented by SRTM 3 arcsecond DSM data covering the regions outside Switzerland.

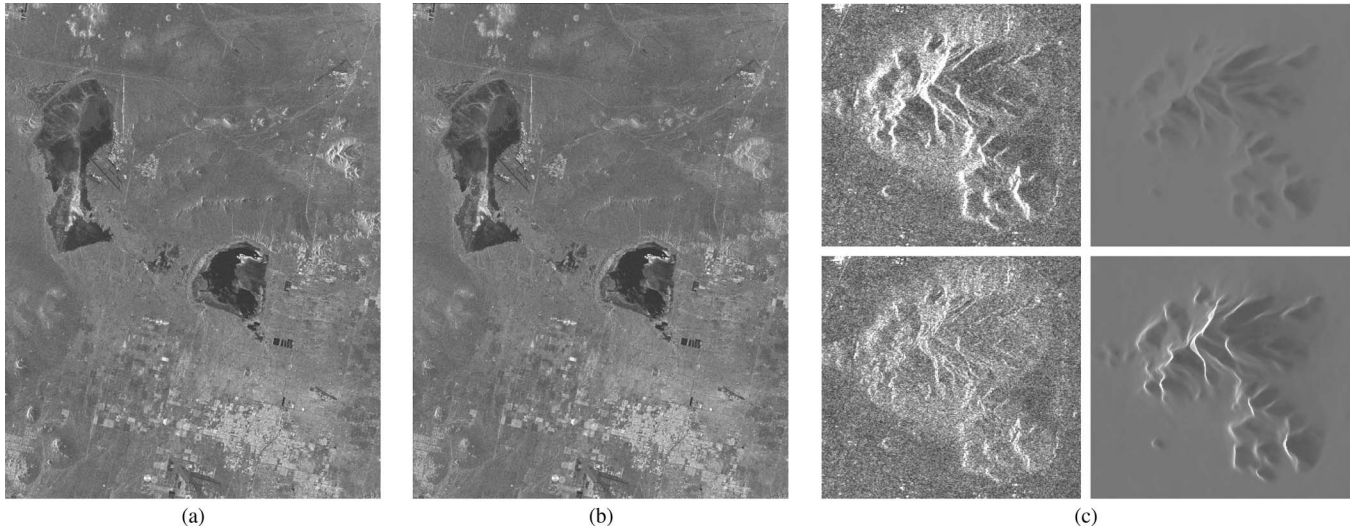


Fig. 2. ERS-2 multilook intensity image of the Mojave Desert before (a) and after (b) radiometric normalization using the pixel-area-based simulated SAR image. (c) (clockwise and starting from top left) a zoom image of a detail from the ERS-2 multilook intensity image of the Mojave Desert [see (a)], the corresponding $\cos(\psi)$ -based image simulation, the pixel-area-based image simulation, and the pixel-area-based σ_{pa}^0 backscatter coefficients.

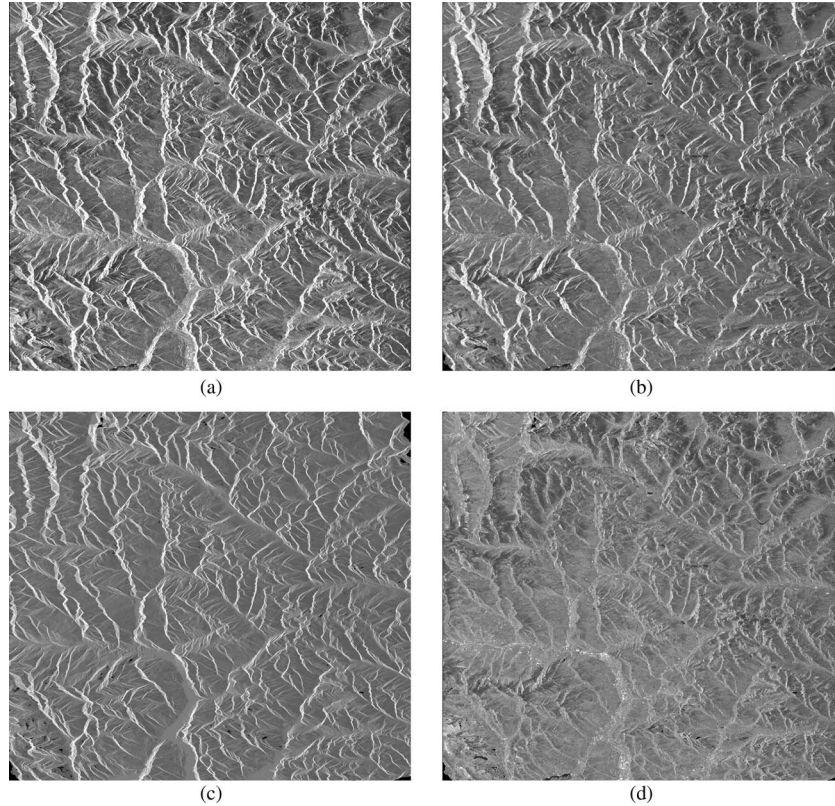


Fig. 3. (a) ERS-2 MLI σ^0 backscatter map of an alpine area in southeastern Switzerland using ellipsoid-based calibration. (b) ERS-2 multilook intensity image (MLI) σ_{\cos}^0 values after radiometric normalization using the DEM-based $\cos(\psi)$ correction approach. (c) Simulated SAR image based on integration of illuminated DEM pixels per range–azimuth coordinate. (d) ERS-2 MLI (σ_{pa}^0) after radiometric normalization using the pixel-area-based simulated SAR image.

The coefficients of the quadratic polynomials that describe the range- and azimuth-varying geocoding offsets between the actual SAR image and the simulated image are given in Table I. Two different simulation methods, i.e., the $\cos(\psi)$ -based and the pixel-area-based simulation of topography-induced radar brightness, were employed. The resulting coefficients are found in Table I(a) and (b), respectively. In addition to the polynomial coefficients, their respective errors, as well as the standard deviations of the model fit, are also given.

B. Radiometric Normalization

In Fig. 4, the performance of the three different radiometric calibration procedures, i.e., ellipsoid-based normalization, $\cos(\psi)$ -based normalization, and pixel-area-based normalization, is quantitatively evaluated for an ERS-2 scene of an alpine region in southeastern Switzerland. The backscatter values are subdivided into classes according to the corresponding local incidence angles. Each box plot represents the median, the 25%, and the 75% percentiles of that particular class, with

TABLE I
ESTIMATED GEOREFERENCING OFFSET POLYNOMIAL COEFFICIENTS AND CORRESPONDING ERRORS AS WELL AS THE STANDARD DEVIATION OF THE MODEL FIT IN RANGE–AZIMUTH FOR THE MOJAVE DESERT DATA SET USING

(a) THE $\cos(\psi)$ -BASED SIMULATED IMAGE AND USING (b) THE PIXEL-AREA-BASED SIMULATED IMAGE AS A REFERENCE

offset poly. coeff	a_0	$a_1(x)$	$a_2(x^2)$	a_0	$a_1(x)$	$a_2(x^2)$
range :	2.41045	1.20996e-04	5.53648e-04	3.07041	-2.50452e-04	2.95323e-04
range err.:	1.10811e-02	5.78788e-06	5.00273e-06	3.45840e-03	1.79884e-06	1.59742e-06
azimuth:	1.59825	-4.74088e-04	-3.61166e-04	-0.00481	-2.18779e-05	3.80772e-06
azimuth err.:	1.74349e-02	9.10663e-06	7.87128e-06	2.05678e-03	1.06981e-06	9.50022e-07
model fit std. dev.	σ			σ		
range:	0.2349 pix.			0.0982 pix.		
azimuth:	0.3696 pix.			0.0584 pix.		

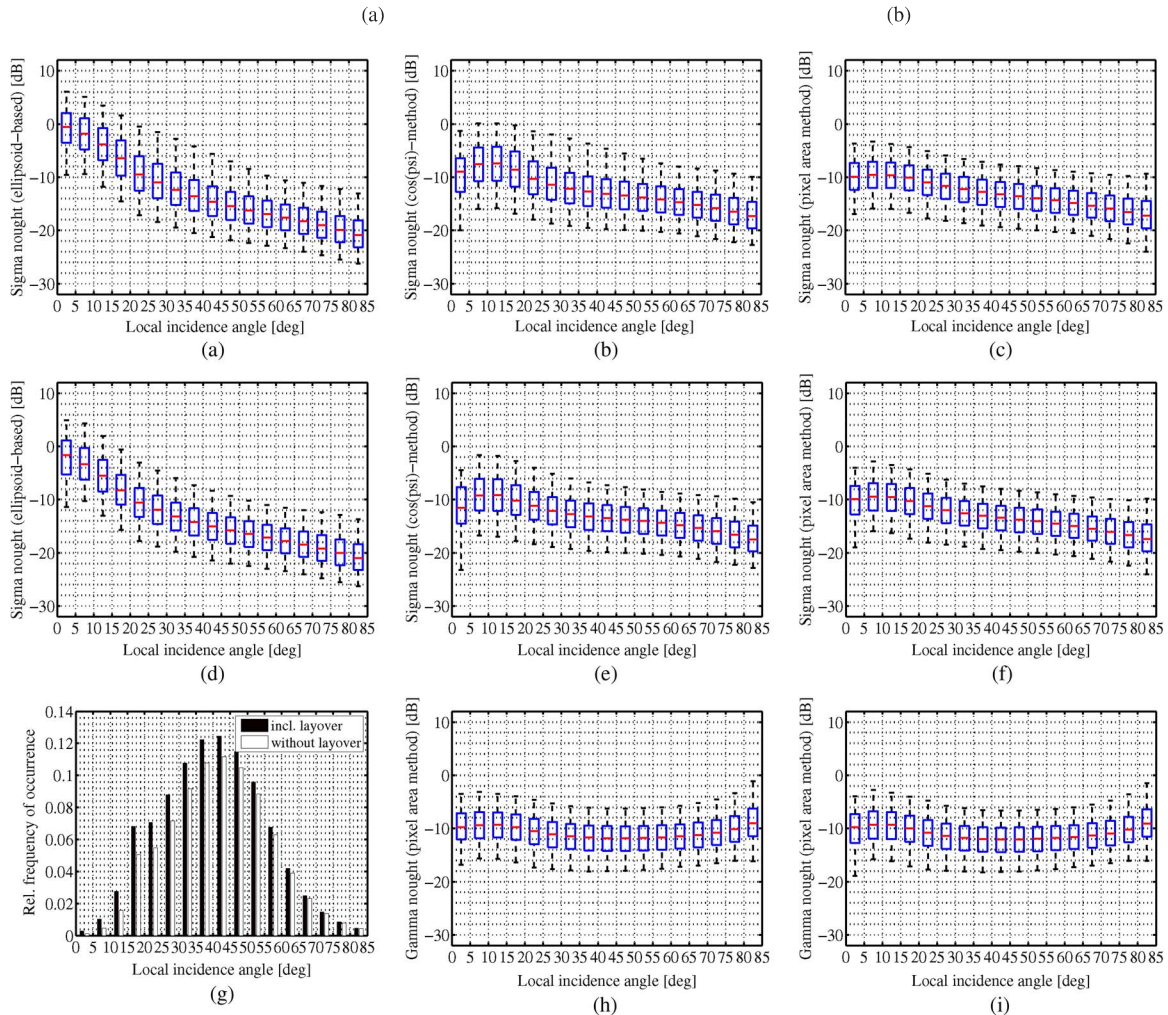


Fig. 4. First row contains box plots (5%, 25%, 50% (median), 75%, and 95% percentiles) according to classes of local incidence angles for the backscatter values of the ERS-2 scene of the alpine region in southeastern Switzerland shown in Fig. 3, including areas affected by layover. (a) Ellipsoid-based σ^0 . (b) $\cos(\psi)$ -based σ_{\cos}^0 . (c) Pixel-area-based σ_{pa}^0 . In the second row, the respective box plots are shown for the same scene, but the layover areas were masked out beforehand. (d) Ellipsoid-based σ^0 . (e) $\cos(\psi)$ -based σ_{\cos}^0 . (f) Pixel-area-based σ_{pa}^0 . The last row contains (g) histograms of relative frequencies of occurrence of SAR pixels according to local incidence angles with and without layover regions, as well as the pixel-area-based γ_{pa}^0 with (h), and without (i) layover-affected areas.

the width of the classes being 5° . The whiskers attached to the boxes indicate the 5% and 95% percentiles. The plots in the first row in Fig. 4 show the distribution of σ^0 values employing, from left to right, the ellipsoid-based radiometric normalization, $\cos(\psi)$ -based radiometric normalization, and pixel-area-based radiometric normalization. In the second row, the respective data evaluation is given only for the nonlayover regions of the same SAR scene. The histogram in Fig. 4(g) contains the relative frequency of occurrence of local incidence angles throughout the SAR image for the two cases: 1) with and 2) without inclusion of layover-affected areas. Finally,

the distributions of the γ_{pa}^0 backscatter values through pixel-area-based normalization with and without layover regions are shown in Fig. 4(h) and (i), respectively.

IV. DISCUSSION

A. Geocoding Refinement

The small patch of the ERS-2 scene depicting the Mojave Desert (see Fig. 2) exhibits very few topography-induced radiometric features only. The importance for accurate modeling of these features based on integration of all illuminated DEM

surface patches is reflected in the much improved estimation errors—by nearly one order of magnitude—when using the pixel-area-based image simulation as a reference.

In this particular and, notably, rather extreme case, it can even be observed that the resulting coefficients of the off-set polynomials are quite different for the two simulations compared. In azimuth, the constant coefficients differ by more than 1.5 samples, and in range, the difference is about 0.6 samples. Judging from the lower estimation errors and the improved standard deviation of the model fit, the pixel-area-based geocoding solution is more robust in this case, where only very few terrain features are present in a SAR image, whereas the $\cos(\psi)$ -based method leads to a biased estimate. This finding is also supported by the fact that if a larger excerpt of the same frame, including more topography, is geocoded, the estimated coefficients tend toward the solution obtained for the pixel-area-based simulation with only the small patch of data.

B. Radiometric Normalization

A visual inspection of the radiometrically normalized backscatter values (see Fig. 3) indicates most strikingly the enhanced radiometric calibration obtained with the pixel-area-based technique. This visual impression is quantitatively underlined by a comparison of the box plots of σ^0 values, which is shown in Fig. 4. While the median backscatter value ranges from 0 dB, for very small local incidence angles, to -21 dB, for large local incidence angles in the case of standard ellipsoid-based normalization, the range of median σ^0 values is reduced to the interval $[-7.5, -17.5]$ dB for the $\cos(\psi)$ -base method, and reduced to $[-9.5, -17.5]$ dB for the pixel-area-based method. In the latter case, the outer quantiles, which mark the range of values where 50% and 90% of the data in a particular bin are contained, span a considerably smaller range (≈ 5 dB and ≈ 12 – 15 dB, respectively) than in the case of the $\cos(\psi)$ -based normalization (≈ 5 – 7 and ≈ 12 – 20 dB, respectively). The improvement is particularly notable for local incidence angles from 0° to 50° . The difference between the two methods is much less pronounced if only nonlayover pixels are considered, as seen in the second row of Fig. 4. If the data are calibrated to γ^0 backscatter coefficients, the median values even stay within $[-9, -12]$ dB.

The bottom line of this analysis is that incorporation of a digital elevation model into the radiometric normalization is indispensable in mountainous areas and that a pixel-area-based normalization is required to obtain an adequate radiometric normalization of layover-affected pixels. It has to be noted that the resolution and the quality of the DEM used for the calculation of the pixel area both have a great influence on the quality of the geocoding refinement and, consequently, also on the quality of the radiometric normalization.

V. CONCLUSION

The advantages of a pixel-area-based simulation of topography-induced variation of radar brightness in SAR images were highlighted using ERS-2 SAR data and digital elevation models. The added value of this pixel-area-based method, compared with conventional methods based on angular relationships, is twofold. First, a more accurate geocoding refinement is obtained since the distinct radiometric features, which are introduced by layover areas and which are crucial to obtain a good correlation between the SAR image and the simulated image in the geocoding process, are now modeled realistically, limited only by the resolution and accuracy of the digital elevation model. The second advantage of the pixel-area-based normalization method compared with the $\cos(\psi)$ -based approach lies in the much improved backscatter normalization in *layover areas*, thereby leading to a smoother appearance of the backscatter map in SAR scenes with distinct topography. Although the resolution remains low in these areas, the improved radiometric normalization aids in detecting features of interest that would otherwise be hidden by topography-induced high backscatter values.

ACKNOWLEDGMENT

ERS-2 data were provided by the European Space Agency. Shuttle Radar Topography Mission digital elevation models provided by the U.S. Geological Survey. DHM25 copyright 2003 by swisstopo.

REFERENCES

- [1] U. Wegmüller, "Automated terrain corrected SAR geocoding," in *Proc. IEEE Geosci. Remote Sens. Symp.*, 1999, vol. 3, pp. 1712–1714.
- [2] A. Löw and W. Mauser, "Generation of geometrically and radiometrically terrain corrected SAR image products," *Remote Sens. Environ.*, vol. 106, no. 3, pp. 337–349, Feb. 2007.
- [3] O. Frey, E. Meier, and D. Nüesch, "Processing SAR data of rugged terrain by time-domain back-projection," in *Proc. SPIE SAR Image Anal., Model., Tech. X*, 2005, vol. 5980, pp. 1–9.
- [4] L. M. H. Ulander, "Radiometric slope correction of synthetic-aperture radar images," *IEEE Trans. Geosci. Remote Sens.*, vol. 34, no. 5, pp. 1115–1122, Sep. 1996.
- [5] D. Small, M. Jehle, E. Meier, and D. Nüesch, "Radiometric terrain correction incorporating local antenna gain," in *Proc. 5th EUSAR*, Ulm, Germany, 2004.
- [6] D. Small, N. Miranda, and E. Meier, "Local incidence angle considered harmful," in *Proc. CEOS SAR Cal/Val Workshop*, Pasadena, CA, Nov. 2009.
- [7] D. Small, N. Miranda, and E. Meier, "A revised radiometric normalisation standard for SAR," in *Proc. IEEE Geosci. Remote Sens. Symp.*, Jul. 2009, vol. 4, pp. 566–569.
- [8] D. Small, N. Miranda, L. Zuberbühler, A. Schubert, and E. Meier, "Terrain-corrected gamma: Improved thematic land-cover retrieval for SAR with robust radiometric terrain correction," in *Proc. ESA Living Planet Symp.*, Bergen, Norway, Jul. 2010, ESA SP-686.
- [9] D. Small, "Flattening gamma: Radiometric terrain correction for SAR imagery," *IEEE Trans. Geosci. Remote Sens.*, vol. 49, no. 8, pp. 3081–3093, Aug. 2011.